Bearing Fault Model for Induction Motor With Externally Induced Vibration

Fabio Immovilli, Claudio Bianchini, Marco Cocconcelli, Alberto Bellini, *Member, IEEE*, and Riccardo Rubini

***Abstract*—This paper investigates the relationship between vibration and current in induction motors operated under external vibrations. Two approaches are usually available to define this relationship. The former is based on airgap variations, while the latter is based on torque perturbation. This paper is focused on the airgap variation model. The ball bearing fault is modeled by contact mechanics. External vibrations often occur in many industrial applications where externally induced vibrations of suitable amplitude cause cyclic radial loading on the machine shaft. The model is validated by experiments, owing to a dedicated test setup, where an external vibration source (shaker) was employed, together with ball bearing alterations in order to decrease the stiffness of the support along the radial direction. To maximize the effects of externally induced vibrations, the frequency chosen was near the flexural resonance of the rotor (determined by finite-element method analysis). The direction of the external vibration is radial with respect to the axis of the electric machine under test. During tests, both stator phase currents and vibration of the machine were sampled. The test setup allowed one to vary the machine speed and load, vibration amplitude, and bearing stiffness (damage level). Radial effects are usually visible only in the case of large failures that result in significant airgap variations, as confirmed by experiments.**

***Index Terms*—Airgaps, ball bearings, condition monitoring, current measurement, fault diagnosis, frequency domain analysis, harmonic analysis, induction motors, modulation, vibration measurement.**

NOMENCLATURE

f_{car}	Fault characteristic frequency.
F_{be}	Stator current fault characteristic frequency.
f	Electric supply frequency.
F_r	Rotor mechanical frequency.
F_{cage}	Cage fault frequency.
F_{outer}	Outer raceway fault frequency.
F_{inner}	Inner raceway fault frequency.
F_{ball}	Ball fault frequency.
M	Rotor mass (comprising shaft and inner races).
F_{weight}	Rotor weight (comprising shaft and inner races).
k_{sphere}	Stiffness of a single sphere.
k_{roller}	Stiffness of a single roller.
Z	Number of ball bearing's spheres.
K_{eq}	Equivalent stiffness of the bearing.
g	Standard gravity.
c	Viscous damping coefficient.

Manuscript received March 30, 2012; revised June 20, 2012; accepted July 24, 2012. Date of publication August 16, 2012; date of current version April 11, 2013.

The authors are with the Dipartimento di Scienze e Metodi dell'Ingegneria, University of Modena and Reggio Emilia, 42122 Reggio Emilia, Italy (e-mail: fabio.immovilli@unimore.it; claudio.bianchini@unimore.it; marco.cocconcelli@unimore.it; alberto.bellini@unimore.it; riccardo.rubini@unimore.it).

Color versions of one or more of the figures in this paper are available online at http://ieeexplore.ieee.org.

Digital Object Identifier 10.1109/TIE.2012.2213566

I. INTRODUCTION

MECHANICAL imbalances and bearing faults account for a large majority of faults in electric machines, particularly in the small–medium power sizes. Electromechanical fault diagnosis in induction machines is an extensively investigated field for cost and maintenance savings. In fact, induction motors are still the most widespread rotating electric machines in industry, mainly because of their low price, ruggedness, and reliability. Many papers can be found in the literature concerning the general condition monitoring of induction machines [1]–[3]. The distribution of failures within the machine subassemblies is reported in many reliability survey papers [4], [5]. A rough classification identifies four classes: bearings faults, stator-related faults, rotor-related faults, and other faults (cooling, connection, and terminal boxes). Depending on the type and size of the machine, bearing fault distribution varies from about 40% to about 90% from large to small machines.

Rolling bearings are used in almost every industrial process involving rotating and reciprocating machinery [6]. In industrial applications, bearings are critical mechanical components: Proper functioning of the equipment depends, to a great extent, on the smooth running of the bearings. Bearing faults that are not detected in time cause malfunction, loss of performance, and reduced efficiency [7], [8] and may even lead to catastrophic failure of the machinery.

Vibration signals are usually employed to detect the presence of mechanical faults in bearings. In many situations, diagnostic methods based on the analysis of the vibration signals have proved their effectiveness [9], [10]. Among the mechanical problems detected by vibration spectra, there are imbalance, misalignment, loose fitting, bent shaft, and bearing localized faults.

Simplified kinematic models of the mechanical components (rolling bearings and meshing gears) are usually employed to simulate fault response of the machine drive train, in order to predict fault frequencies [11], [12].

Recently, many research activities have been focused on the diagnosis of bearing faults by motor current signal analysis (MCSA) [13]–[15]. In many cases, mechanical signals cannot be directly acquired, e.g., in harsh environments or because the application is in a noisy environment with shocks and external vibrations. Under such conditions, electric signal measurements

would be preferable as they are more immune to mechanical disturbances.

Noninvasive fault diagnosis should ideally detects faults at the early stage, to allow for scheduled maintenance, which minimizes system downtime. Under these circumstances, fault signature components feature a very small amplitude that is usually buried in noise and can lead to false positive detection [16]. The use of suitable signal processing techniques is required to efficiently extract the fault signatures from raw signals.

In order to detect fault signature data, vibration and current signals are usually processed to retrieve the information of interest: A short outline of the most common signal processing techniques used for fault detection is reported hereafter. Statistical scalar indicators are used to provide a single parameter characterizing the health status of a mechanical component. Usually, the monitored parameter is the vibration signal, and the most used indicators are the root-mean-square (rms) value of the vibration velocity, the crest factor, and the kurtosis. The rms is an indicator of the energy lost due to dissipative phenomena: Indicative rms thresholds are suggested in [17] and [18]. The crest factor is defined as the ratio between the maximum peak and the rms of the vibration signal. This indicator states the significance of impulsive phenomena (such as those correlated with an impact between bearing elements) with respect to the rms value of the signal. The crest factor becomes unreliable as damage progresses because, during damage progression, the amplitude of the peaks associated with impacts decreases while the rms of vibration increases. The kurtosis can be seen as the deviation from the standard probability distribution of a real-valued random variable. In the case of a healthy bearing, white noise is expected with a normal Gaussian distribution. A fault introduces specific components that depart from the normal distribution, thus increasing the kurtosis value. More powerful statistical approach and feature extraction algorithms are also employed, particularly for fault classification purposes [19].

Frequency domain analysis is the most important technique used so far in literature. In most cases, the presence of a damage introduces impacts related to the motion of the system. If the rotation of the machine is constant, then the impacts are periodic and the frequency of train of impacts could be detected in the spectrum of the signal. Usually, a fault on a moving element modulates the amplitude of vibration signal with a frequency which is characteristic of the damage [20]. Envelope analysis can be used to effectively retrieve the fault signature components, e.g., Hilbert transform [21]. The Hilbert transform allows one to compute the *analytical signal* which is a complex-valued function where the real part is the original signal and the imaginary part is the Hilbert transform of the original signal. The analytic representation is a generalization of the phasor concept that allows one to conveniently separate the effects of amplitude modulation and phase modulation.

In the presence of nonstationary signals, transient impacts may occur at unknown time intervals; thus, the resulting signal is commonly nonperiodic. In this case, the Fourier analysis is no longer suitable since the time information is lost. Time–frequency techniques can be used to overcome this problem: short-time Fourier transform and wavelet transform. In the wavelet analysis, the signal is no longer decomposed as a sum of harmonics—as in the Fourier transform—but as a sum of specific functions called mother wavelet whose characteristic size could be changed [22]. Wavelet analysis is particularly useful when dealing with transient operation [23], [24].

The use of current and/or voltage signal ideally constitutes a noninvasive method to bring information necessary to the diagnosis system and, thus, to ensure an effective online monitoring of the electric machine [25], [26]. However, the physical link between bearing faults and current signatures is still debated.

This paper compares the use of vibration and current signal for bearing fault detection in induction machines, with particular reference to the imbalance/airgap variation fault model.

The paper contribution is the theoretical analysis of the physical link between bearing faults and vibration spectrum components and the development of a bearing dynamic model to predict fault frequencies and airgap variation for cage faults and loss of stiffness on roller bearings. To this aim, a bearing model based on contact mechanics will be presented and applied to the case of external harmonic excitation. Experiments were conducted to evaluate the model and verify simulation results. A test setup was constructed that allows one to monitor vibration and current signals on a machine with externally induced vibrations. The external vibration source is an electromagnetic (EM) shaker, and the direction of vibration is radial with respect to the shaft axis of the electric machine under test.

This paper is organized as follows. Section II reviews the relationship between vibration and current components presented in literature. Section III outlines the proposed kinematic fault model of the bearing in case of external harmonic excitation. Section IV presents the simulation results obtained with the contact mechanics model. Section V presents the results of finite-element (FE) method (FEM) modeling of the flexural modes of the test rotor, together with an experimental characterization by means of a frequency sweep on the shaker. Section VI reports the experimental results for test run at different vibration levels and bearing stiffness, with data comparison against the simulation results. Section VII presents some final remarks and conclusions.

II. Vibration and Current Correlation

There are a number of papers dealing with the detection and diagnosis of electromechanical faults based on MCSA in induction motors [25]–[28]. The physical mechanism that links vibrations to motor current spectral components is still debated and is presented in the literature according to different approaches.

According to the first approach, the vibration component at one of the fault characteristic frequencies $f_{\rm car}$ acts on the electric machine as a torque ripple that produces a speed ripple [29]. Hence, the vibration is seen as a torque component that generates in the current a chain of components at frequencies F_{be}

$$F_{be} = |f \pm k\, f_{\rm car}| \tag{1}$$

where k is an integer.

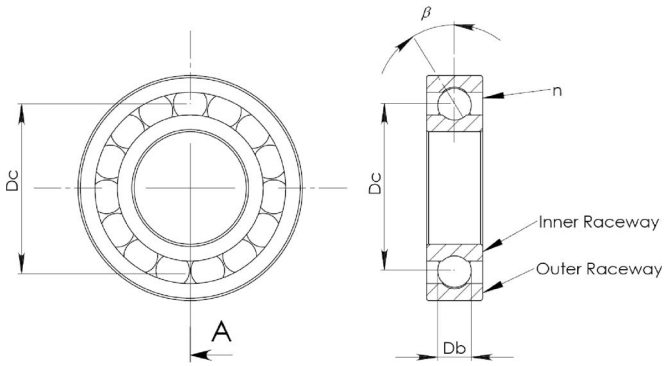

Fig. 1. Bearing structure and parameters.

According to the second approach, the effect of the vibration component on the current is modeled as a static eccentricity that is represented as the sum of forward and backward rotating eccentricities [30].

In [31], a unifying approach is presented in order to define a model of stator current induced by defect in rolling bearing elements. Here, the two aforementioned physical effects are considered separately. The effect of radial rotor displacement is modeled as an airgap length variation, i.e., as an airgap permeance variation, that results in a variation of the flux density in the airgap and, consequently, on the stator current.

In any case, vibrations generate modulation in the stator currents at predictable frequencies F_{be} related to the mechanical frequencies and electrical supply frequency (1).

Radial bearings consist of two concentric rings or races, outer and inner, separated by balls or rollers (Fig. 1). Rolling elements are bound by a cage: a component that maintains a constant angular pitch between adjacent rolling elements and prevents any contact.

Localized faults will produce characteristic vibration frequency components. These bearing fault frequencies are a function of the bearing geometry, the operating speed, and whether the outer or the inner ring is fixed to the frame. Characteristic vibration frequencies can be computed from the bearing's physical dimensions (Fig. 1). In particular, if the outer ring is fixed

$$F_{\text{cage}} = \frac{1}{2} F_r \left(1 - \frac{D_b \cos\beta}{D_c}\right) \tag{2}$$

$$F_{\text{outer}} = \frac{n}{2} F_r \left(1 - \frac{D_b \cos\beta}{D_c}\right) \tag{3}$$

$$F_{\text{inner}} = \frac{n}{2} F_r \left(1 + \frac{D_b \cos\beta}{D_c}\right) \tag{4}$$

$$F_{\text{ball}} = \frac{D_c}{D_b} F_r \left[1 - \left(\frac{D_b \cos\beta}{D_c}\right)^2\right] \tag{5}$$

where D_b stands for the ball diameter, D_c for the pitch diameter, n for the number of rolling elements, and β for the ball contact angle (Fig. 1). Bearing characteristic fault frequencies usually are also provided by the manufacturer for diagnostic purposes.

Table I reports the corresponding vibration-related components according to [31], for both approaches to fault modulation of stator currents. Results are extended to the cage fault case, that is the topic of this paper.

The correlation between the vibration level and the magnitude of the current sideband is tested experimentally, varying the vibration level and frequency [32].

According to the eccentricity model, vibration effects on machine currents are caused by airgap variations; hence, machine current modulation effects are related to displacement. Because of electromechanical filtering effects (due to the rotor inertia and winding inductance), MCSA is more sensitive to low-frequency phenomena [33]. The attenuation of bearing fault current modulation is enhanced in the case of higher fault characteristic frequency; hence, MCSA can detect only defects characterized with relatively low characteristic frequency [33]. In summary, it is still very difficult to retrieve bearing fault components by MCSA. The aim of this paper is to investigate the airgap variation model by artificially creating a fault at cage frequency and simultaneously excite the machine at the flexural resonance of the rotor in order to amplify the airgap variation effects. In the following paragraphs, the bearing fault model will be developed and presented, together with experimental characterization of the machine rotor and results obtained from external shaker excitation experiment.

III. Harmonic Excitation Fault Model

From a mechanical point of view, the loss of spheres translates in an increased clearance between the contacting bearing components. This causes a reduction of the stiffness and increases the mobility of the shaft in the radial direction. This usually leads to the appearance of a peak at F_{cage} in the vibration spectrum. With reference to the fixed outer ring, the periodicity of the passage of the unsupported sector has the same frequency of the cage rotation (2), since the cage itself keeps fixed the relative position of the rolling elements. If the external radial load is constant along a fixed direction (e.g., in the case of a pulley connected to the motor), the model is the same as shown in Fig. 2(a), where the frequency of the stiffness variation is identical to that of the cage, because the unsupported area is aligned to the radial force direction once per revolution. If the external radial load is a harmonic motion (e.g., shaker vibration), it acts on the bearing with a push–pull excitation, and the unsupported area is aligned to the force direction twice per revolution. Hence, the effect of the varying stiffness is seen at $2F_{\text{cage}}$. This second case is shown in Fig. 2(b). The basic model described by (2)–(5) is no longer satisfactory in the presence of an external harmonic load; hence, a more detailed one will be implemented (Fig. 3).

In order to keep the model simple, only three force components will be considered:

1) the force supplied by the shaker;
2) the weight of the rotor and shaft;
3) the variable stiffness distribution of the bearing.

A single-degree-of-freedom lumped parameter model is assumed, as shown in Fig. 3. In particular, the rotor is represented

TABLE I
VIBRATION-RELATED COMPONENTS IN THE STATOR CURRENT SPECTRUM

	Model based on eccentricity	Model based on torque fluctuations
Outer raceway defect	$f \pm k\,F_{outer}$	$f \pm k\,F_{outer}$
Inner raceway defect	$f \pm F_r \pm k\,F_{Inner}$	$f \pm k\,F_{inner}$
Ball defect	$f \pm F_{cage} \pm k\,F_{ball}$	$f \pm k\,F_{ball}$
Cage defect	$f \pm F_{cage}$	$f \pm k\,F_{cage}$

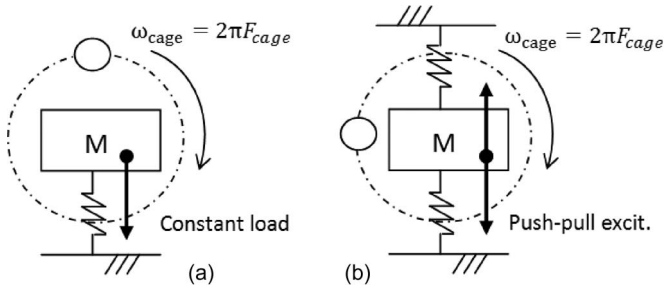

Fig. 2. Kinematic model of the rotating cage fault in the case of (left) constant radial load on the bearing and (right) push–pull harmonic excitation.

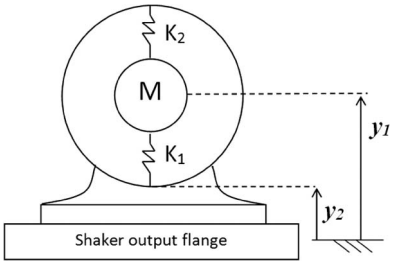

Fig. 3. Kinematic model of the bearing stiffness in supporting the rotor of the machine.

by a suspended mass M (comprising rotor, shaft, and inner races) connected with the stator by means of a spring K_1 whose value depends on the angular position of the cage and will be described later in this section. Finally, the stator/frame is subjected to the excitation of the shaker. Only displacements along the vertical direction are considered, i.e., one independent motion $y_1(t)$ is assumed as a Lagrangian parameter, while $y_2(t)$ represents the instant position of the shaker's output flange. Since the shaft is supported all around by means of the cage and spheres, a second spring K_2 is considered, which acts when the mass M is translating upward while the stator is going downward. Nominally, K_1 and K_2 are equal for a healthy bearing; they differ from each other when a fault is present (e.g., rolling element removal). In the construction of the model, lumped damping elements parallel to the springs are introduced to stabilize the solver. Regarding Fig. 3, forces and dampers are not graphically represented for the sake of clarity.

The shaker provides a harmonic excitation, represented by

$$y_2(t) = A_{\text{shaker}} \cos(2\pi f_{\text{shaker}} t + \Phi_{\text{shaker}}) \tag{6}$$

where A_{shaker}, f_{shaker}, and Φ_{shaker} are the amplitude, the frequency, and the phase of the excitation displacement, respectively. The first two parameters are known as they are set points of the shaker control loop. The phase is arbitrarily chosen in the simulation. The rotor's own weight force is constant and directed along the vertical direction, as the gravitational

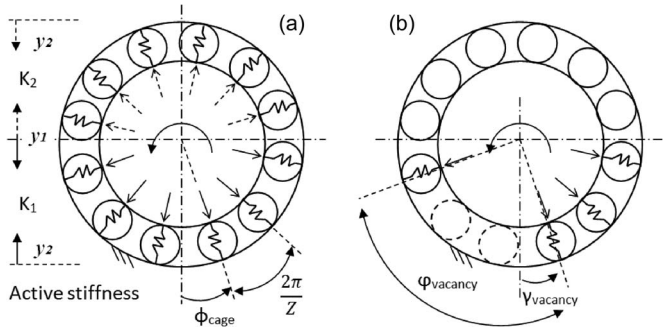

Fig. 4. Load distribution among spheres in a healthy bearing. (a) Maximum coverage. (b) Minimum coverage.

acceleration is opposite to the chosen positive displacement direction in the reference frame

$$F_{\text{weight}} = -Mg. \tag{7}$$

Even in a healthy bearing, the radial stiffness of the ball bearing changes periodically with the shaft rotation. In fact, assuming a bearing load zone of about 180°, the number of loaded spheres at a given time is a function of the cage rotation angle. A similar effect appears in gear transmissions, where the stiffness of the teeth changes according to the covering factor.

In this model, only the spheres are considered deformable, thus contributing to the bearing stiffness; inner and outer rings are considered nondeformable. Furthermore, taking into account the geometric distribution, stiffness is not only dependent upon the number of spheres present but also on their relative positions. Fig. 4(a) shows how each sphere contributes to the equivalent stiffness of the bearing. The equivalent stiffness is the sum of each contribution (as the modeled springs are in parallel configuration), while the single contribution depends on the angle Φ_{cage} between the angular position of the sphere and the reference axis. Contact mechanics theory is then applied to the system. According to Hertz's contact theory, the sphere radial deformation is proportional to the contact force raised to the 2/3 power. In the case of cylindrical rollers, there is a linear relationship between contact force and deformation. The force contribution of each sphere along the load direction can be expressed as

$$Q = \sum_{i}^{Z} P_i \cos\left(\Phi_{\text{cage}} + i\frac{2\pi}{Z}\right) \tag{8}$$

where P_i is the force exerted by the generic ith sphere. The ratio between the ith and the jth force is assumed to be equal to the ratio of the corresponding displacement of the spheres via Hooke's law

$$\frac{F_i}{F_j} = \frac{\epsilon_i}{\epsilon_j} \cdot \frac{\cos^{\frac{2}{3}}(\phi_j)}{\cos^{\frac{2}{3}}(\phi_i)} \tag{9}$$

where the generic $\phi_k = (\Phi_{\text{cage}} + k(2\pi/Z))$. It must be noticed that, in a healthy bearing, the sphere configuration repeats with a $2\pi/Z$ period (where Z is the number of spheres). During this period, a sphere (dotted line) can leave the load zone, thus altering the equivalent stiffness, as shown in Fig. 4(b). Including (9) in (8) leads to the computation of the equivalent stiffness

$$K_{\text{eq}} = k_{\text{sphere}} \cdot \sum_{i}^{Z} \delta_{lj} \cos^{\frac{5}{2}} \left(\Phi_{\text{cage}} + i\frac{2\pi}{Z} \right) \tag{10}$$

where k_{sphere} is assumed to be equal to Young's module of steel. The δ_{lj} is the Kronecker delta, with l and j being its conditions, expressed as

$$l = \text{sign} \left[\cos \left(\Phi_{\text{cage}} + i\frac{2\pi}{Z} \right) \right] \tag{11}$$

$$j = \text{sign}(\Delta y_0 + y_2 - y_1) \tag{12}$$

where the function $\text{sign}[x]$ returns $+1$ if the argument is positive, -1 if the argument is negative, and 0 if otherwise and Δy_0 is the distance $(y_1 - y_2)$ in the reference condition (motor and shaker stopped). With reference to Fig. 4(a), (10) can be easily explained: When the shaft is moving downward with respect to the reference condition, only the spheres below the horizontal line of symmetry are loaded. In this case, the sign of (12) is positive, and only the spheres lying in the bottom part (force components with solid line) give a contribution to the equivalent stiffness since the sign of (11) is positive in this region. On the other hand, when the shaft is moving upward with respect to the neutral position, (12) is negative, and only the spheres lying in the upper part (force components with dotted line) give a negative output to (11); then, they are counted in the computation of the respective equivalent stiffness. In summary, because of the construction geometries, each equivalent stiffness of the bearing is defined only for compression loads: Hence, the equivalent stiffness became equal to K_1 when the shaft is moving downward, while it is equal to K_2 when it is moving upward.

The condition of (10) takes into account whenever a sphere leaves the load zone.

When N spheres are removed from the bearing, the unsupported vacancy zone can be modeled as a superimposition of a cyclic phenomenon with the same rotating frequency of the cage. Fig. 4(b) shows an example with two spheres removed. The amplitude of the resulting vacancy zone can be written as

$$\varphi_{\text{vacancy}} = (1 + N)\frac{2\pi}{Z}\Phi_{\text{cage}}. \tag{13}$$

An initial phase γ_{vacancy} of the vacancy location with reference to the vertical axis may be chosen but is assumed to be zero in the simulation without loss of generality. Equation (10) should be corrected to take into account the effect of the vacancy.

By combining (13) with (10), the equivalent stiffness of the faulty bearing can be obtained

$$K_{\text{eq}} = k_{\text{sphere}} \cdot \sum_{i}^{Z} \delta_{lj} \nu_i \cos^{\frac{5}{2}} \left(\Phi_{\text{cage}} + i\frac{2\pi}{Z} \right) \tag{14}$$

where

$$\nu_i = \left(i\frac{2\pi}{Z} \right) \notin \left[\gamma_{\text{vacancy}}; N\frac{2\pi}{Z} + \gamma_{\text{vacancy}} \right]. \tag{15}$$

Equation (15) returns 0 if the term $i2\pi/Z$ belongs to the given interval and 1 if otherwise.

The equation of the system dynamics can then be expressed as

$$M\ddot{y_1} + c(\dot{y_1} - \dot{y_2}) + K_{\text{eq}}(y_1 - y_2) = F_{\text{weight}} \tag{16}$$

where, as mentioned before, the viscous damping coefficient c is assumed proportional to a fraction of the equivalent stiffness for stabilization purposes only.

The model can be extended to the case of cylindrical roller bearings as well. According to Hertz's contact theory, a linear relationship exists between contact force and deformation for cylindrical elements. Consequently, (14) becomes

$$K_{\text{eq}} = k_{\text{roller}} \cdot \sum_{i}^{Z} \delta_{lj} \nu_i \cos^{2} \left(\Phi_{\text{cage}} + i\frac{2\pi}{Z} \right). \tag{17}$$

IV. Simulation Results

A model of the system, based on (14) and (16), was then computed in MATLAB-Simulink environment. The viscous damping coefficient c is assumed proportional to the equivalent stiffness (0.1%), and the stiffness of a single sphere k_{sphere} is set equal to Young's module of steel (210 000 N/mm^2). In order to calculate the expected results, the input parameters for the model were set according to the experimental setup (e.g., SKF 1204 bearing characteristic dimensions, motor rotating speed, and shaker excitation frequency and amplitude).

Fig. 5 shows the block diagram of the model. The radial vibration of the rotor with respect to the stator was computed, and the resulting waveform is plotted in Fig. 6. Demodulation of this radial vibration signal reveals a dominant component that is equal to the second harmonic of the rotational frequency of the cage (Fig. 7). These results will be experimentally assessed in the following paragraphs, starting with the analysis of the rotor flexural mode shapes and frequencies, to identify the suitable test conditions for the subsequent experiment on the electrodynamic shaker.

V. Rotor Characterization: FEM Modeling and Frequency Sweep

Prior to the experiment on the electrodynamic shaker, the machine's rotor was dynamically characterized to identify its flexural mode shapes and frequencies. The machine rotor (Fig. 8) was modeled in a 3-D computer-aided-design environment, and its flexural mode shapes and frequencies were computed owing to FE analysis. The rotor lamination diameter is 77 mm with a length of 90 mm; the shaft diameter is 25 mm with an overall length of 270 mm. The model was meshed into 77 518 solid elements with 3.5-mm dimension, and then, a frequency analysis considering the bearing restraints was performed using

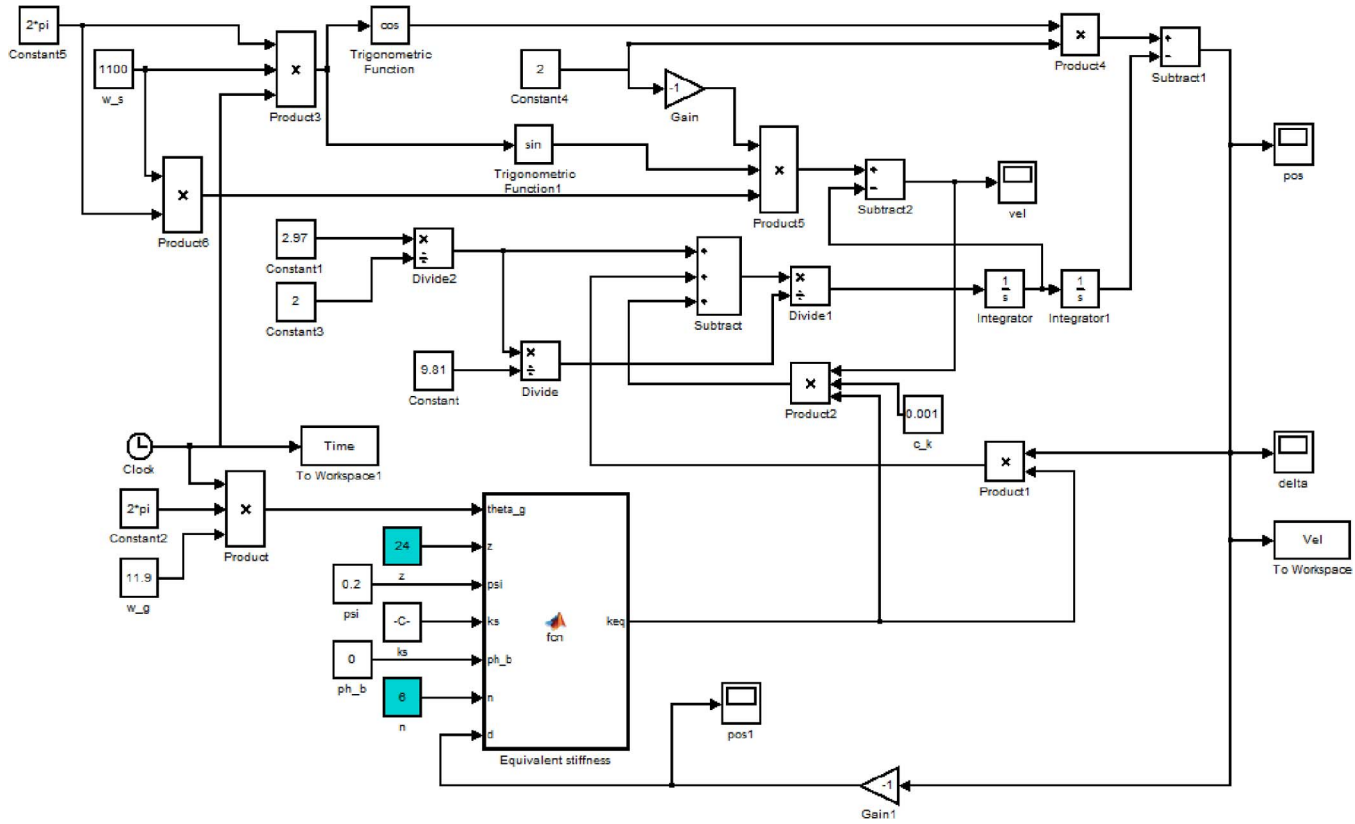

Fig. 5. Simulink model of the bearing system with cage fault.

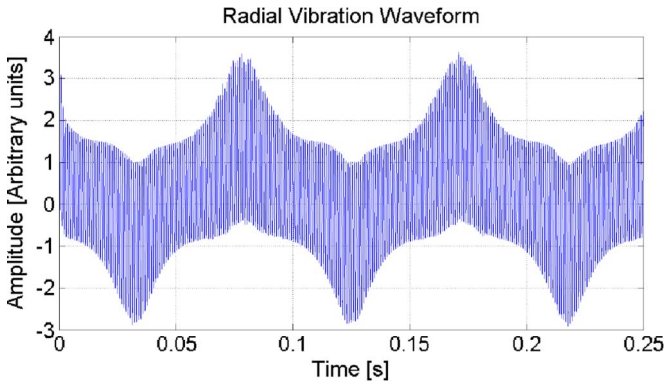

Fig. 6. Simulation results: Radial vibration waveform of the shaft, due to faulty bearing.

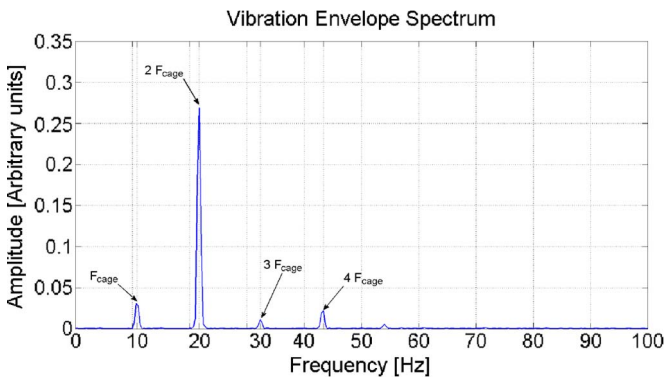

Fig. 7. Simulation results: Vibration spectrum of the shaft due to faulty bearing.

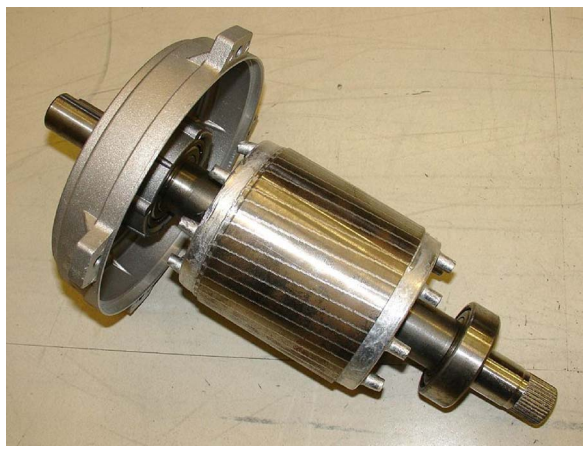

Fig. 8. Picture of the machine rotor, with bearings and end caps.

a direct sparse solver. The first and second flexural mode shapes of the rotor are shown in Figs. 9 and 10, and the resonance frequencies are 1053.3 and 2282.6 Hz, respectively.

The machine resonances were also experimentally characterized, by means of a sine wave frequency sweep test on the electrodynamic shaker (Fig. 16). The motor was mounted on the output flange of the shaker and then radially loaded by a sine sweep excitation. The sine sweep spans the 0–3000-Hz frequency range. Two accelerometers [one on the frame of the motor and the other directly mounted on the surface of the flange; Fig. 13(b)] are used to compute the frequency response function (FRF) of the entire electric machine.

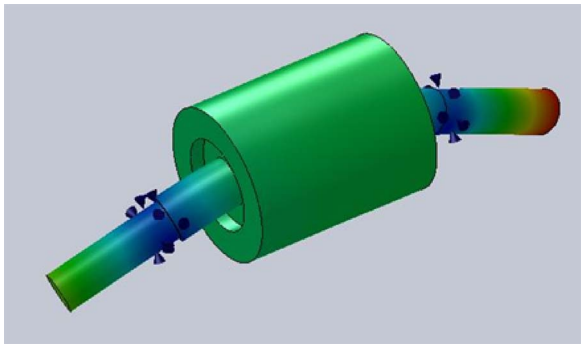

Fig. 9. Rotor's first mode shape deformed view.

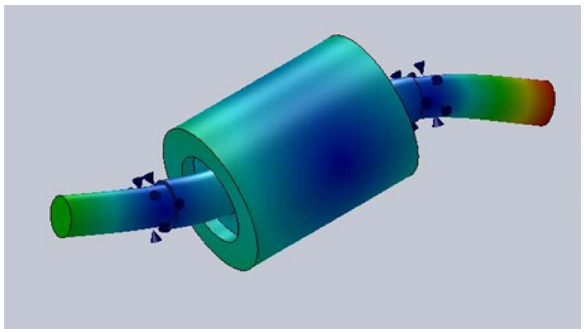

Fig. 10. Rotor's second mode shape deformed view.

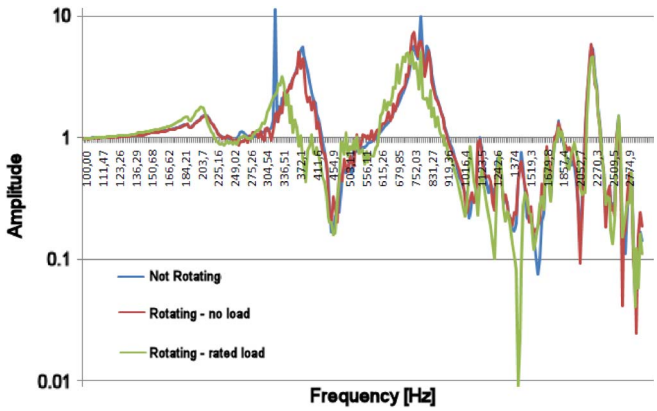

Fig. 11. Frequency response of the machine under test.

Fig. 11 shows three superimposed curves which refer to three FRFs at different working conditions of the motor: stopped (blue), rotating without load torque (red), and under load torque (green). The FRF curves need interpretation to correctly identify the resonance frequencies: The higher peaks at 372 and 752 Hz change dependently of the working condition of the motor, while characteristic resonance frequencies are independent.

Among these considerations, the choice of the suitable experimental resonance frequencies is guided by the results of the FEM analysis of the rotor. Referring to Fig. 11, the second resonance frequency is clearly evident at 2200 Hz. The first mode shape at around 1100 Hz has a node in correspondence of the bearing position, and then, it appears as an antiresonance minimum in the FRF. Both values are close to the FEM results (1053.3 and 2282.6 Hz): This is a further confirmation that

TABLE II
MACHINE ROTOR FLEXURAL RESONANCE FREQUENCIES

Mode	Calculated	Experimental
First	1053.3 Hz	1100 Hz
Second	2282.6 Hz	2200 Hz

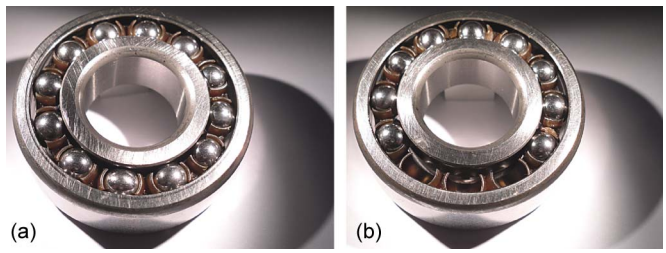

Fig. 12. Photographs of the bearings used in the experiments. (a) Healthy bearing. (b) Bearing with spheres removed.

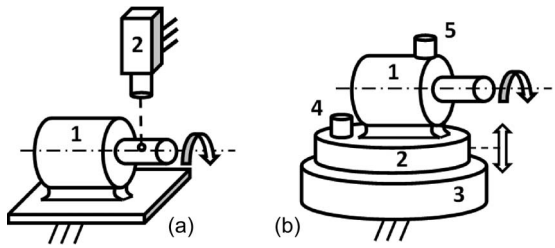

Fig. 13. Schematic diagrams of the experimental setups. (a) Constant load setup: (1) Motor and (2) laser vibrometer. (b) Harmonic excitation setup: (1) Motor, (2) mounting plate, (3) shaker, (4) reference accelerometer, and (5) test accelerometer.

the lower peaks at 372 and 752 Hz are probably related to the resonance frequencies of the whole test rig structure (i.e., EM shaker and the induction motor) instead of the natural frequencies of the motor only.

Computed and experimental resonance frequencies are summarized in Table II.

VI. EXPERIMENTAL RESULTS

A small induction machine was used to assess the airgap variation model of the faulty bearing. Two sets of front bearings were employed: One is healthy, while the other was artificially faulted by removing an increasing number of spheres (Fig. 12). In order to maximize the effect of an airgap variation in the motor and to simulate different damage severity, an increasing number of adjacent spheres were removed from the bearing (the higher the number of spheres removed, the higher the severity of the fault).

A preliminary test was conducted to assess the presence of a cage fault frequency oscillation on the shaft of the machine with constant load and no vibration [Fig. 13(a)].

The motor was fastened to a bench (Fig. 14), and the radial displacement vibration of the rotor was measured using a laser vibrometer (POLYTEC OFV-505). Fig. 15 shows the spectrum of the radial displacement velocity in the case of six balls removed from the bearing: F_{cage} is clearly present together with F_r as a consequence of the imbalance caused by the asymmetrical stiffness of the faulty bearing.

Fig. 14. Laser vibrometer setup.

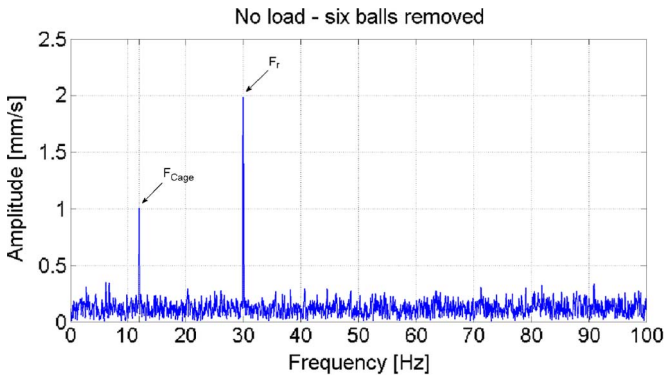

Fig. 15. Spectrum of the shaft radial displacement velocity in the case of faulty bearing without external excitation (measured with laser vibrometer).

The main experimental setup [Fig. 13(b)] is detailed as follows.

1) The machine under test is a 1-kW three-phase induction machine, with 60-Hz rated frequency, wye connection windings, 28 rotor bars, and two pole pairs.
2) The machine was operated at constant volts-per-hertz ratio at output loads between zero and the rated load. A power inverter, operated at a switching frequency of 13 kHz, generates the supply voltages.
3) An air-cooled EM brake (based on eddy currents) was devised to provide a variable output load for the machine.
4) The external excitation is provided by an air-cooled shaker Data Physics V-400. The induction machine is fixed to the header of the shaker by three M10 screws. The shaker provided a dwell excitation at the first and second rotor flexural mode frequencies with vibration levels equal to 2 g.

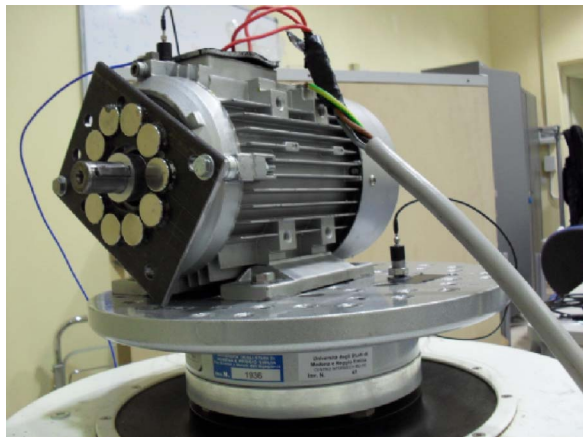

Fig. 16. Photograph of the test setup used for bearing fault detection.

TABLE III
EXPECTED CHARACTERISTIC FREQUENCIES FOR MACHINE OPERATION AT 60 Hz

Frequency	No load torque	Rated load torque
f	60 Hz	60 Hz
F_r	30 Hz	27.3 Hz
F_{cage}	11.9 Hz	10.8 Hz
$f \pm F_{cage}$	48.1 ÷ 71.9 Hz	49.2 ÷ 70.8 Hz

5) A triaxial vibration sensor was used to pick up vibrations on the machine bearing cap: An integrated circuit piezoelectric accelerometer model 356A01 with sensitivities equal to 5.22 mV/g (X-axis), 4.27 mV/g (Y-axis), and 5.00 mV/g (Z-axis) and a frequency range from 0.3 to 15 000 Hz.
6) SKF 1204 self-aligning ball bearing was employed for easy dismantling and access to inner components. The bearing stiffness in the radial direction was altered by removing up to six rolling elements to recreate a loss of stiffness fault with characteristic frequency equal to F_{cage}.

The test setup allows one to measure motor stator currents, rotor speed, and vibration signals, as well as the exciting frequency/amplitude of the shaker (Fig. 16). Machine currents, voltages, speeds, and vibration signals were sampled at 25 kHz. Overall, the test rig is similar to the one proposed in [34], where the external excitation was generated by an unbalanced auxiliary motor. In both cases, the resulting excitation is a variable radial load acting on the machine bearings. Two test runs were conducted with supply frequency f equal to 60 Hz, varying the load on the machine: The expected mechanical and electrical frequencies are summarized in Table III. The aforementioned conditions were employed to induce large imbalances due to operation near the flexural resonance frequencies (identified in the previous section) combined with reduced stiffness of the bearings.

Fig. 17 shows the vibration signal of the machine running under a load with different harmonic excitations, displaying amplitude modulation. Fig. 18 shows the spectrum of the vibration envelope. The envelope of the vibration signal was computed as in [33] using a simple algorithm without complex preprocessing (filtration) of the acquired signal. When the machine is excited at the first flexural resonance frequency of the shaft, the spectrum shows strong modulating harmonics at F_{cage} and $2F_{\text{cage}}$, in agreement with the proposed fault model

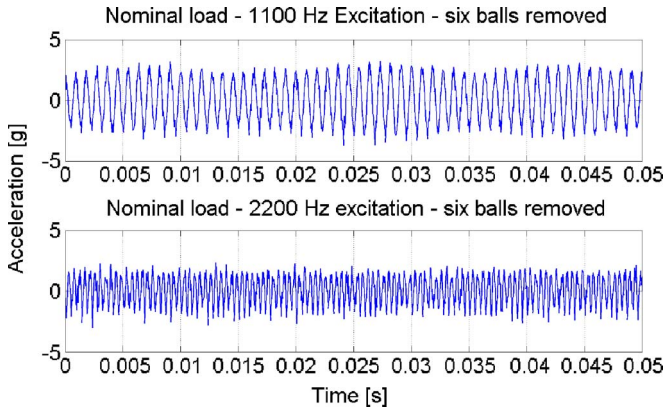

Fig. 17. Vibration signal of the machine with different harmonic excitations.

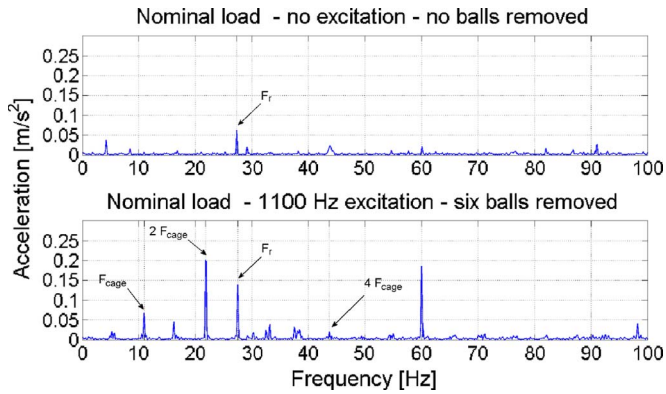

Fig. 18. Vibration envelope spectrum: Machine running at 60 Hz under rated load torque.

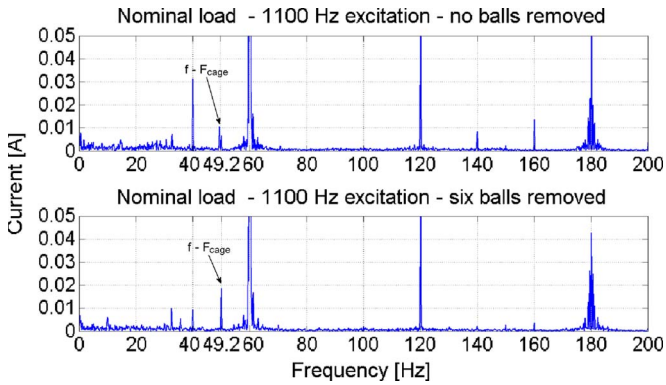

Fig. 19. Stator current spectrum: Machine running at 60 Hz under rated load torque.

and simulations. The rise of the F_r component testifies an increased imbalance of the rotor, as expected by the deformation of the first flexural mode shape.

Fig. 19 shows the spectrum of one stator current, the others having a similar behavior. The characteristic harmonic at $f - F_{\text{cage}}$ appears when the machine is excited at the first flexural resonance frequency of the shaft. The amplitude of the $f - F_{\text{cage}}$ harmonic increases when the bearing stiffness is reduced by removing an increasing number of rolling elements (increased damage severity). In this configuration, the current signal is a more robust indicator, as its modulations are not influenced by the particular excitation method (constant radial loading versus push–pull harmonic loading). In the case of the current signal, the rotating eccentricity caused by the cage fault is always at F_{cage}; thus, the results are independent from external mechanical excitation and operating conditions. This is opposed to the vibration analysis where the $2F_{\text{cage}}$ harmonic was dominant in the case of shaker push–pull harmonic excitation.

VII. Conclusion

Fault diagnosis in electric machines operating under a high level of ambient vibration is an open topic. This is a common situation in many industrial applications where externally induced vibrations of sufficient amplitude cause cyclic radial loading on the machine shaft (e.g., industrial vibrators and conveyors). Electromechanical fault diagnosis in electric machines is traditionally developed assuming a constant radial load on the bearings. This paper has dealt with the fault diagnosis of roller bearings applied to an induction machine operated under external vibration, employing vibration analysis and MCSA according to the airgap variation model. The key results of the work are summarized as follows.

1) A detailed kinematic bearing fault model, based on contact mechanics, was developed and applied to simulate the system response in the case of external harmonic excitation.
2) A model of roller bearing faults based on airgap variation model was applied for the relationship between current and vibration in induction machines.
3) A dedicated test setup was realized to validate the analytical model. The experimental setup allows one to monitor vibration and current signals on a machine with externally induced vibrations.
4) Simulation results were confirmed by experimental results, with the identification of fault signatures in both current and vibration spectra.

The investigation allows stating a few general assumptions.

1) Radial effects leading to airgap variation are usually visible only in the case of large failures that result in appreciable loss of stiffness.
2) As reported by previous papers, the use of current signals for mechanical fault detection is effective only for those faults whose characteristic frequency is lower than the supply frequency, such as cage frequency. Hence, it is possible to use current signals as reliable media to detect bearing faults only in specific operating conditions.
3) Under external harmonic excitation, current and vibration signals behave differently. In the current signal, the rotating eccentricity caused by the cage fault is always at F_{cage}; thus, the results are independent from external mechanical excitation and operating conditions. In the vibration signal analysis, the $2F_{\text{cage}}$ harmonic was dominant in the case of shaker push–pull harmonic excitation. In the case of external harmonic excitation, MCSA is not affected by the excitation method (constant radial loading or push–pull harmonic loading), while vibration signal analysis requires a suitable analysis of the working and mounting conditions in order to correctly interpret the spectrum modulations.

REFERENCES

[1] S. Nandi, H. A. Toliyat, and X. Li, "Condition monitoring and fault diagnosis of electrical motors—A review," *IEEE Trans. Energy Convers.*, vol. 20, no. 4, pp. 719–729, Dec. 2005.

[2] A. Bellini, F. Filippetti, C. Tassoni, and G. A. Capolino, "Advances in diagnostic techniques for induction machines," *IEEE Trans. Ind. Electron.*, vol. 55, no. 12, pp. 4109–4126, Dec. 2008.

[3] A. Garcia-Perez, R. de Jesus Romero-Troncoso, E. Cabal-Yepez, and R. Osornio-Rios, "The application of high-resolution spectral analysis for identifying multiple combined faults in induction motors," *IEEE Trans. Ind. Electron.*, vol. 58, no. 5, pp. 2002–2010, May 2011.

[4] O. V. Thorsen and M. Dalva, "A survey of faults on induction motors in offshore oil industry, petrochemical industry, gas terminals, and oil refineries," *IEEE Trans. Ind. Appl.*, vol. 31, no. 5, pp. 1186–1196, Sep./Oct. 1995.

[5] A. H. Bonnett, "Root cause AC motor failure analysis with a focus on shaft failures," *IEEE Trans. Ind. Appl.*, vol. 36, no. 5, pp. 1435–1448, Sep./Oct. 2000.

[6] C. Bianchini, F. Immovilli, M. Cocconcelli, R. Rubini, and A. Bellini, "Fault detection of linear bearings in brushless ac linear motors by vibration analysis," *IEEE Trans. Ind. Electron.*, vol. 58, no. 5, pp. 1684–1694, May 2011.

[7] G. Curcuru', M. Cocconcelli, F. Immovilli, and R. Rubini, "On the detection of distributed roughness on ball bearings via stator current energy: Experimental results," *Diagnostyka*, vol. 51, no. 3, pp. 17–21, 2009.

[8] L. Frosini and E. Bassi, "Stator current and motor efficiency as indicators for different types of bearing faults in induction motors," *IEEE Trans. Ind. Electron.*, vol. 57, no. 1, pp. 244–251, Jan. 2010.

[9] R. Rubini and U. Meneghetti, "Application of the envelope and wavelet transform analysis for the diagnosis of incipient faults in ball bearings," *Mech. Syst. Signal. Process.*, vol. 15, no. 2, pp. 287–302, Mar. 2001.

[10] J. R. Stack, T. G. Habetler, and R. G. Harley, "Fault-signature modeling and detection of inner-race bearing faults," *IEEE Trans. Ind. Appl.*, vol. 42, no. 1, pp. 61–68, Jan./Feb. 2006.

[11] N. Sawalhi and R. Randall, "Simulating gear and bearing interactions in the presence of faults: Part I. The combined gear bearing dynamic model and the simulation of localised bearing faults," *Mech. Syst. Signal Process.*, vol. 22, no. 8, pp. 1924–1951, Nov. 2008.

[12] N. Sawalhi and R. Randall, "Simulating gear and bearing interactions in the presence of faults: Part II: Simulation of the vibrations produced by extended bearing faults," *Mech. Syst. Signal Process.*, vol. 22, no. 8, pp. 1924–1951, Nov. 2008.

[13] A. Ibrahim, M. El Badaoui, F. Guillet, and W. Youssef, "Electrical signals analysis of an asynchronous motor for bearing fault detection," in *Proc. IEEE IECON*, Nov. 2006, pp. 4975–4980.

[14] L. Sun and B. Xu, "An improvement of stator current based detection of bearing fault in induction motors," in *Proc. IEEE IAS Annu. Meeting*, New Orleans, LA, Sep. 2007, pp. 2277–2281.

[15] M. Blodt, M. Chabert, J. Regnier, and J. Faucher, "Mechanical load fault detection in induction motors by stator current time–frequency analysis," *IEEE Trans. Ind. Appl.*, vol. 42, no. 6, pp. 1454–1463, Nov./Dec. 2006.

[16] S. Choi, B. Akin, M. Rahimian, and H. Toliyat, "Performance-oriented electric motors diagnostics in modern energy conversion systems," *IEEE Trans. Ind. Electron.*, vol. 59, no. 2, pp. 1266–1277, Feb. 2012.

[17] *Evaluation of Machine Vibration by Measurements on Non-Rotating Parts*, ISO 10816-1, 1995.

[18] R. D. Almeida, S. D. S. Vincente, and L. Padovese, "New technique for evaluation of global vibration levels in rolling bearings," *Shock Vib.*, vol. 9, no. 4/5, pp. 225–234, 2002.

[19] J. Yu, "Local and nonlocal preserving projection for bearing defect classification and performance assessment," *IEEE Trans. Ind. Electron.*, vol. 59, no. 5, pp. 2363–2376, May 2012.

[20] J. Stack, R. Harley, and T. Habetler, "An amplitude modulation detector for fault diagnosis in rolling element bearings," *IEEE Trans. Ind. Electron.*, vol. 51, no. 5, pp. 1097–1102, Oct. 2004.

[21] R. Randall, J. Antoni, and S. Chobsaard, "The relationship between spectral correlation and envelope analysis in the diagnostics of bearing faults and other cyclostationary machine signals," *Mech. Syst. Signal Process.*, vol. 15, no. 5, pp. 945–962, Sep. 2001.

[22] D. Newland, *An Introduction to Random Vibrations, Spectral and Wavelet Analysis*. New York: Dover, 2005.

[23] J. Cusido, L. Romeral, J. Ortega, J. Rosero, and A. Garcia Espinosa, "Fault detection in induction machines using power spectral density in wavelet decomposition," *IEEE Trans. Ind. Electron.*, vol. 55, no. 2, pp. 633–643, Feb. 2008.

[24] Y. Gritli, C. Rossi, L. Zarri, F. Filippetti, A. Chatti, and D. Casadei, "Double frequency sliding and wavelet analysis for rotor fault diagnosis in induction motors under time-varying operating condition," in *Proc. IEEE Int. SDEMPED*, Sep. 2011, pp. 676–683.

[25] I. Georgakopoulos, E. Mitronikas, and A. Safacas, "Detection of induction motor faults in inverter drives using inverter input current analysis," *IEEE Trans. Ind. Electron.*, vol. 58, no. 9, pp. 4365–4373, Sep. 2011.

[26] V. Choqueuse, M. Benbouzid, Y. Amirat, and S. Turri, "Diagnosis of three-phase electrical machines using multidimensional demodulation techniques," *IEEE Trans. Ind. Electron.*, vol. 59, no. 4, pp. 2014–2023, Apr. 2012.

[27] J. R. Stack, T. G. Habetler, and R. G. Harley, "Fault classification and fault signature production for rolling element bearings in electric machines," *IEEE Trans. Ind. Appl.*, vol. 40, no. 3, pp. 735–739, May/Jun. 2004.

[28] J. R. Stack, T. G. Habetler, and R. G. Harley, "Bearing fault detection via autoregressive stator current modeling," *IEEE Trans. Ind. Appl.*, vol. 40, no. 3, pp. 740–747, May/Jun. 2004.

[29] M. Blodt, D. Bonacci, J. Regnier, M. Chabert, and J. Faucher, "On-line monitoring of mechanical faults in variable-speed induction motor drives using the Wigner distribution," *IEEE Trans. Ind. Electron.*, vol. 55, no. 2, pp. 522–533, Feb. 2008.

[30] C. M. Riley, B. K. Lin, T. G. Habetler, and R. R. Schoen, "A method for sensorless on-line vibration monitoring of induction machines," *IEEE Trans. Ind. Appl.*, vol. 34, no. 6, pp. 1240–1245, Nov./Dec. 1998.

[31] M. Blodt, P. Granjon, B. Raison, and G. Rostaing, "Models for bearing damage detection in induction motors using stator current monitoring," *IEEE Trans. Ind. Electron.*, vol. 55, no. 4, pp. 1813–1822, Apr. 2008.

[32] F. Immovilli, C. Bianchini, M. Cocconcelli, A. Bellini, and R. Rubini, "Currents and vibrations in asynchronous motor with externally induced vibration," in *Proc. IEEE Int. SDEMPED*, Sep. 2011, pp. 580–584.

[33] F. Immovilli, A. Bellini, R. Rubini, and C. Tassoni, "Diagnosis of bearing faults in induction machines by vibration or current signals: A critical comparison," *IEEE Trans. Ind. Appl.*, vol. 46, no. 4, pp. 1350–1359, Jul./Aug. 2010.

[34] C. Riley, B. Lin, T. Habetler, and G. Kliman, "Stator current-based sensorless vibration monitoring of induction motors," in *Proc. Conf. 12th Annu. APEC*, Feb. 1997, vol. 1, pp. 142–147.

Fabio Immovilli was born in Italy on March 11, 1981. He received the M.S. and the Ph.D. degrees in mechatronic engineering from the University of Modena and Reggio Emilia, Reggio Emilia, Italy, in 2006 and 2011, respectively.

In 2009, he was a Visiting Scholar in the Power Electronics, Machines and Control Group, University of Nottingham, Nottingham, U.K. Since 2011, he has been a Research Fellow of electric converters, machines, and drives with the Dipartimento di Scienze e Metodi dell'Ingegneria, University of Modena and Reggio Emilia. He is the holder of one international industrial patent. His research interests include electric machine diagnosis, power converters, machines for energy conversion from renewable energy sources, and thermoacoustics.

Claudio Bianchini was born in Italy on September 9, 1974. He received the S.B. degree in mechatronic engineering, the M.S. degree in management engineering, and the Ph.D. degree from the University of Modena and Reggio Emilia, Reggio Emilia, Italy, in 2002, 2006, and 2010, respectively.

During 2008, he was an Honorary Scholar at the University of Wisconsin, Madison. Since 2010, he has been a Research Fellow of electric converters, machines, and drives with the Dipartimento di Scienze e Metodi dell'Ingegneria, University of Modena and Reggio Emilia. He is the holder of one international patent. His research interests include electric machines and drives, and static power conversion for renewable energy.

Marco Cocconcelli was born in Italy on November 9, 1977. He received the M.S. degree in mechanical engineering and the Ph.D. degree in applied mechanics from the University of Bologna, Bologna, Italy, in 2003 and 2007, respectively.

In 2007, he joined the University of Modena and Reggio Emilia, Reggio Emilia, Italy, as a Research Fellow of applied mechanics, where he is currently with the Dipartimento di Scienze e Metodi dell'Ingegneria. He is an Editorial Assistant for the *International Journal of Theoretical and Applied Mechanics MECCANICA*. He is the holder of one international patent. His research interests include bearing diagnostics, kinematics, and dynamics of planar mechanisms, and kinetic models in gait analysis.

Dr. Cocconcelli is a member of the Italian Association of Theoretical and Applied Mechanics (AIMETA), the International Institute of Acoustics and Vibration, and the Italian Society of Clinical Movement Analysis (SIAMOC).

Alberto Bellini (S'96–M'99) was born in Italy in 1969. He received the M.S. degree in electronic engineering and the Ph.D. degree in computer science and electronic engineering from the University of Bologna, Bologna, Italy, in 1994 and 1998, respectively.

From 1999 to 2004, he was with the University of Parma, Parma, Italy. During 2000, he was an Honorary Scholar at the University of Wisconsin, Madison. Since 2004, he has been with the University of Modena and Reggio Emilia, Reggio Emilia, Italy, where he is currently an Assistant Professor of electric machines and drives. He is the author or coauthor of more than 80 papers and one textbook, and he is the holder of three industrial patents. His research interests include power electronics, signal processing for audio and industrial applications, and electric drive design and diagnosis.

Dr. Bellini is a member of the Italian Association of Converters, Electrical Machines and Drives (CMAE). He serves as an Associate Editor of the IEEE TRANSACTIONS ON INDUSTRIAL ELECTRONICS. He was the recipient of the First Prize Paper Award from the Electric Machines Committee of the IEEE Industry Applications Society in 2001.

Riccardo Rubini received the M.S. degree in mechanical engineering and the Ph.D. degree in applied mechanics from the University of Bologna, Bologna, Italy.

He was a Visiting Scholar at the Laboratory "Heuristique et Diagnostic des Systèmes Complexes," Université de Technologie de Compiègne, Compiègne, France. He is currently an Associate Professor of mechanics of machines with the University of Modena and Reggio Emilia, Reggio Emilia, Italy. He is the holder of one international patent. His research interests are focused in the fields of machine dynamics and monitoring and diagnostic techniques for mechanical components.

Dr. Rubini is a member of the Italian Association of the Theoretical and Applied Mechanics (AIMETA), the International Federation for the Promotion of Mechanism and Machine Science, Italy, and the Italian Society of Clinical Movement Analysis (SIAMOC).